Chemistry & Biology
Article

Halogen Bonding Controls Selectivity of FRET Substrate Probes for MMP-9

Isabelle Tranchant,[1] Laura Vera,[1] Bertrand Czarny,[1] Mehdi Amoura,[1] Evelyne Cassar,[1] Fabrice Beau,[1] Enrico A. Stura,[1] and Vincent Dive[1,*]
[1]CEA, iBiTec-S, Service d'Ingénierie Moléculaire des Protéines (SIMOPRO), Labex LERMIT, CE-Saclay, 91191 Gif sur Yvette Cedex, France
*Correspondence: vincent.dive@cea.fr
http://dx.doi.org/10.1016/j.chembiol.2014.01.008

SUMMARY

Matrix metalloproteinases (MMPs) are a large family of zinc-dependent endoproteases that catalyze cleavage of extracellular matrix and nonmatrix proteins. MMPs play a role in tissue remodeling, and their uncontrolled activity is associated with number of diseases, including tumor metastasis. Thus, there is a need to develop methods to monitor MMP activity, and number of probes has been previously described. The key problem many probes encounter is the issue of selectivity, since 23 human MMPs, despite playing different physiological roles, have structurally similar active sites. Here, we introduce the halogen bonding concept into the probe design and show that the probe containing iodine exhibits an unprecedented selectivity for MMP-9. We provide structure-based explanation for the selectivity, confirming that it is due to formation of the halogen bond that supports catalysis, and we highlight the value of exploring halogen bonding in the context of selective probe design.

INTRODUCTION

Human matrix metalloproteinases (MMPs) constitute a family of 23 structurally related extracellular/cell-surface-anchored zinc endoproteases (Fanjul-Fernández et al., 2010). MMPs cleave extracellular matrix proteins and thereby mediate both normal and pathological tissue remodeling processes (Mott and Werb, 2004; Sternlicht and Werb, 2001). Their functions extend beyond the matrix, and MMPs act as regulators of diverse processes by cleaving nonmatrix extracellular proteins (Morrison et al., 2009; Parks et al., 2004). Consequently, there have been substantial efforts to detect and inhibit uncontrolled MMP activity under various pathological conditions and to exploit them as biomarkers or therapeutic targets (Fingleton, 2007; Fu et al., 2008). Various protocols have been used to detect MMP activity. The simplest is based on the use of synthetic fluorescence resonance energy transfer (FRET) substrates as probes that fluoresce on cleavage. However, such substrates do not display substantial specificity, despite significant efforts to develop selectivity; this limits their value because any cleavage activity cannot be attributed unambiguously to a particular MMP (Akers et al., 2012; Jabaiah and Daugherty, 2011; Jiang et al., 2004; Kridel et al., 2001). The inability to discriminate between different MMPs also hinders the design of highly selective inhibitors (Yiotakis and Dive, 2008). These difficulties are, in large part, due to the substantial structural similarities between the active sites of the various MMPs (Devel et al., 2010). Here, we describe the exploitation of the unique properties of halogens to mediate diverse and highly specific interactions within the active sites of proteins to allow discrimination between closely related MMPs.

RESULTS

We used the peptide sequence of a fluorogenic peptide commonly used to monitor MMP activity as the basis for our FRET substrate probe. In this substrate probe, the P_1' position is occupied by a leucine residue that partially fills the deep S_1' channel in the active sites of all MMPs. The unusual shape of the MMP S_1' cavity can be exploited to develop new probes with long and bulky side chains in the P_1' position; these side chains can be adapted to fit the S_1' cavity of a particular MMP (Figure 1A). The presence of unusual amino acids in the substrate sequence may also contribute to selectivity by preventing cleavage by other proteases possessing shallower S_1' cavities. While the catalytic efficiency of a set of five MMPs to cleave such probes was high (compounds **1** to **4**; k_{cat}/K_M: $1 \times 10^5\ M^{-1} \cdot s^{-1}$ to $6 \times 10^5\ M^{-1} \cdot s^{-1}$), these probes discriminated only poorly the different MMPs (Figure 1B).

Several carbonyl groups of the protein polypeptide chain point into the cavity of the MMP S_1' pocket. As halogens can interact with electron-rich oxygen atoms such as those in carbonyl groups (i.e., halogen bonding or X-bonding) (Auffinger et al., 2004; Parisini et al., 2011), we evaluated substrate probes with P_1' phenylalanine analogs halogenated in the paraposition (X = F, Cl, Br, I). The catalytic efficiency of MMP-9 to cleave these probes increased in the order F < Cl < Br < I (compounds **5** to **8**) (Figure 1C), which correlated with the predicted halogen X-bond strength (Politzer et al., 2010). Probe **8** was cleaved 23 times more efficiently than probe **5** (Table S1 available online) and also more efficiently than probes **1–4** by MMP-9. Assayed on five MMPs, probe **8** also displayed a better selectivity profile (Figure 1C). These observations reveal that a single atom, pointing toward the S_1' cavity and positioned away from the catalytic zinc ion, can affect transition-state stabilization in this enzymatic system. The ability of probe **8** to discriminate between MMP-2 and MMP-9, in particular, is remarkable because their enzyme cavities are structurally highly similar. For MMP-2, the replacement of fluorine by iodine in the probe only increases the catalytic efficiency 3-fold, while, for MMP-9, this modification results

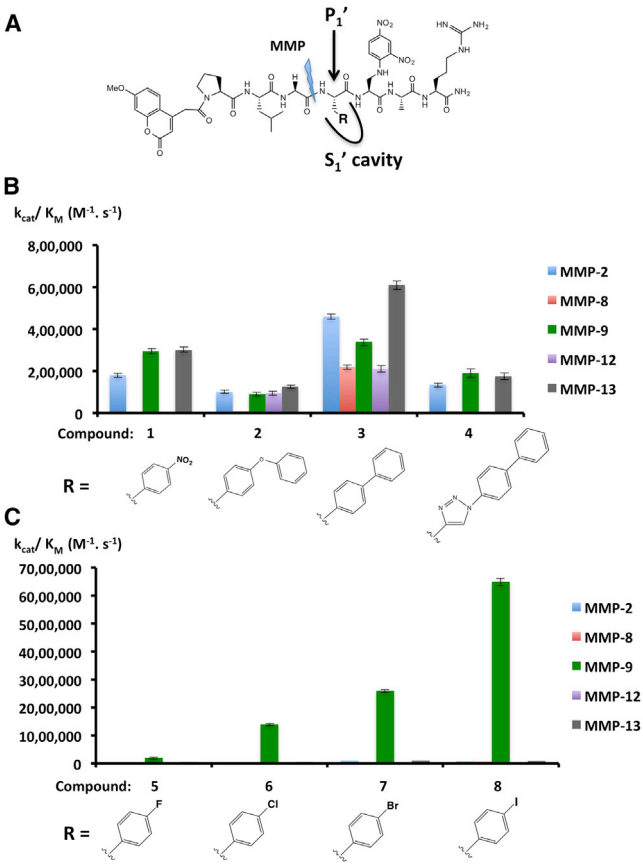

Figure 1. Chemical Structure and Selectivity of Probe Substrates 1 to 8 for MMPs

(A) Generic chemical structure of substrate probes; the blue arrow indicates the peptide bond cleaved by MMPs, and the simple arrow indicates the P_1' position of the probe substrate, with the its side chain plugging in the S_1' cavity; the bold letter R refers to the side chain of the probes.

(B) Increasing the size of the side chain (indicated by the bold letter R) in the P_1' position involved a modest improvement of the probe substrate selectivity (compounds **1** to **4**) toward MMPs (color coded).

(C) In contrast, the nature of the halogen atom in compounds **5** to **8** is a determinant for probe selectivity and allowed the identification of a probe substrate selective for MMP-9. Data are means ± SEM.

See also Tables S1 and S4.

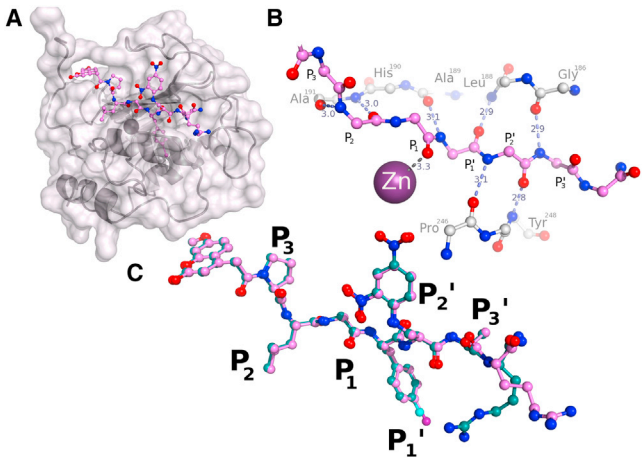

Figure 2. Crystal Structures of MMP-9 Complexes with Probe Substrates 5 and 8

(A) Surface representation of an MMP-9 catalytic domain with probe substrate **8** indicated by a pink ball and stick, the P_1' p-iodo-phenylalanine side chain entering the S_1' subsite can be seen through the transparent protein surface. Oxygen, red; nitrogen, blue.

(B) Probe substrate **8** establishes seven hydrogen bonds with the MMP-9 active site, with the carbonyl of the scissile peptide bond interacting with the zinc ion.

(C) Superimposition of probe substrates **5** and **8** as bound to MMP-9 shows overlap between probes, except for the phenyl ring of probe **8**, which penetrates slightly deeper into the pocket, and, because the carbon-iodine bond is longer than the carbon-fluorine bond, the iodine (indicated in purple; fluorine is indicated in cyan) is positioned further down in the S_1' cavity.

See also Table S2.

in a 23-fold increase of the catalytic efficiency (Table S1). In addition, for MMP-2, the highest catalytic efficiency was observed for the probe containing bromine than for the probes containing the other halogens. Thus, despite the substantial similarity between the active sites of MMP-2 and MMP-9, the use of halogens allows clear discrimination between these two MMPs.

The iodine atom is larger than the fluorine atom and may therefore fill the S_1' cavity of MMP-9 better, leading to the observed difference in enzymatic efficiencies. However, the results with probes **1** to **4** are inconsistent with this explanation: bulky groups on probes **1** to **4** that fill this cavity equally well were not selective (Figure 1B). It is, therefore, likely that the observed differences are associated with specific interactions involving the halogen atoms.

Crystallization proved to be difficult, but we were able to determine the crystal structures of MMP-9 in complex with probes **5** and **8**. Both probes were crystallized with an inactive mutant of the minicatalytic domain of MMP-9, in which the catalytic glutamate residue was replaced by an alanine ($Glu^{227} \rightarrow Ala^{227}$) to avoid probe cleavage. This mutation has been widely used to crystallize MMP-9 (Tochowicz et al., 2007), as it also prevents protease autolysis without affecting the protein structure. The two MMP-9 complexes were crystallized in the same lattice with two molecules in the asymmetric unit (Table S2). The MMP-9:**8** complex is a structure of MMP-9 with an intact peptide substrate spanning the entire active site from subsites S_3 to S_3' (Figure 2A). The probe adopts an elongated conformation, forming a β strand within the active site stabilized by seven hydrogen bonds, with the scissile peptide pointing above the zinc atom (Figure 2B), near the Ala^{227} residue (Figures S1C and S1D), and with the para-iodo-Phe residue side chain pointing into the S_1' cavity (Figure 2A). The iodine atom in this cavity is in close proximity to a water molecule, so the $I—O_W$ distance (O_W represents the oxygen atom in water) is short (2.4 and 2.71 Å for molecules A and B, respectively), much shorter than the sum of their van der Waals radii (3.55 Å) (Figure 3A; Figures S1A and S1B); and the C-$I—O_W$ angles are 163° and 172° (for molecules A and B, respectively) (Figure 3A; Figures S1A–S1D; Table S3). The O_W is also in hydrogen bond distance of the carbonyl oxygen atom of the Arg^{249} peptide bond: the $O_W—OC_{Arg}$ distance is 2.48 and 2.78 Å for molecules A and B, respectively (Figure 3A;

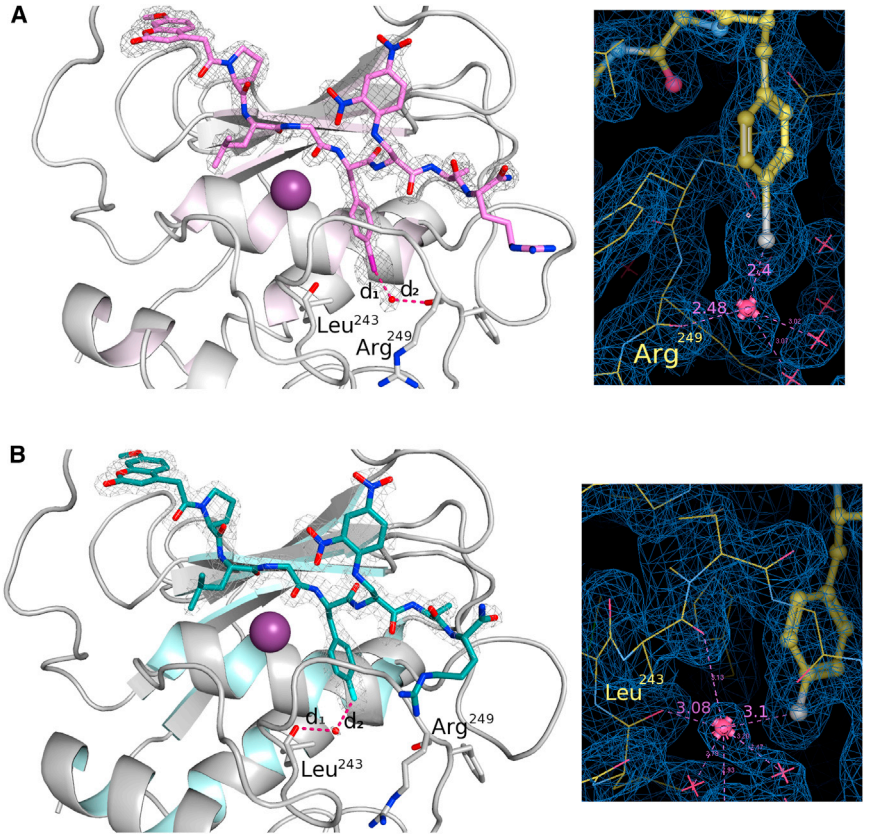

Figure 3. Details of the Interactions Involving the Halogens in the MMP-9 Active Site

(A) Left: molecular representation of the crystal structure of the MMP-9:**8** complex with the red dashed line showing the I (purple)—O_W(red ball)—H bridge involving the carbonyl of Arg^{249}. Probe **8** is indicated by a pink ball and stick, and the zinc atom is indicated as a big purple sphere. Right: electron density map around the iodine atom (gray ball) and the water molecule (pink crossed sphere). The d_1 and d_2 distance values (left panel) are reported. Oxygen, red; nitrogen, blue.

(B) Left: molecular representation of the crystal structure of the MMP-9:**5** complex showing the fluorine atom (cyan) relative to a water molecule (red sphere), which is within hydrogen bonding distance from the Leu^{243} carbonyl. The zinc atom is indicated as a big purple sphere. Right: electron density map around the fluorine atom (gray ball) and the water molecule (pink crossed sphere). The d_1 and d_2 distance values (left panel) are reported. See also Figure S1 and Table S3.

Figures S1A–S1D; Table S3). Thus, the water molecule forms a stabilizing bridge between the iodine of probe **8** and the carbonyl oxygen of Arg^{249} in MMP-9 (iodine-water-hydrogen [I-W-H] bridge, with a distance $I—O_W—OC_{Arg249}$ = 4.4 Å [longer dashes indicate noncovalent bonds; shorter dashes indicate covalent bonds]). Other geometric measures characterizing this halogen-water-hydrogen bridge are reported in Table S3. The values fit well with those previously reported for I-W-H bridges formed between proteins and small ligands (Zhou et al., 2010).

To determine whether this halogen X-bonding is specific for the iodine atom, we also looked at the MMP-9:**5** complex. The structures MMP-9:**8** and MMP-9:**5** were isomorphous, and superimposing the structures of the two protein complexes revealed a near-perfect fit (Figure 2C). The positions of the two probes coincide with each other with only minor deviations, except for the p-iodo-Phe and p-fluoro-Phe side chains. The iodine atom of probe **8** penetrates deeper than the fluorine of probe **5** due to the longer iodine-carbon bond length and a slightly different positioning of the benzyl ring (Figure 2C). With the fluorine probe, as for the iodine probe, a water molecule was observed near the halogen, but at a different position; as a result, the $F—O_W$ distances were 3.1 to 3.18 Å in molecules A and B and thus longer than the sum of the F and O_W van der Waals radii (2.75 Å) (Table S3). This is consistent with the positive electrostatic potential (the σ-hole) of fluorine being smaller than those of other halogens, limiting its interactions with electron-rich atoms (Politzer and Murray, 2013). The water molecule closest to the fluorine atom establishes a hydrogen bond with the carbonyl of Leu^{243}, Tyr^{245}, and Ala^{242}, instead of Arg^{249} (Figure 3B; Figures S1E and S1F). In the MMP-9:**8** complex, the electron density map shows overlap between the electron clouds of the iodine atom and those of the oxygen atom of the interacting water molecule, a feature not shared by the fluorine probe 5 (Figures 3A and 3B).

The FRET probe described in this study can be used in various conditions in vitro to detect MMP-9 activity. When probe **8** was assayed on a large set of MMPs, it still displayed selectivity toward MMP-9 (Figure 4). Under the experimental conditions used, in 30 min, almost all of the probe **8** was cleaved by MMP-9, whereas, for other MMPs, only a faint cleavage was observed (Figure 4; Figure S2). MMP-9 cleaves probe **8** with a k_{cat}/K_M value of $6.5 \times 10^6\ M^{-1} \cdot s^{-1}$, which is among the highest catalytic efficiencies reported to date for an MMP FRET substrate probe. Therefore, assays with probe **8** have a detection threshold of 0.5 fmol of MMP-9 (reaction time, 30 min and in a volume of 100 μl). The kinetic parameters for the cleavage of probes **8** and **5** by MMP-9 were determined: the presence of the iodine atom rather than a fluorine atom increases both the K_M and k_{cat} values (Table S4). We also studied the cleavage of probe **8** by five cathepsins, as these enzymes are commonly overexpressed in pathological tissues (Verdoes et al., 2013). Capthesins S, B, and V did not cleave the probe under the experimental conditions used, while cathepsins K and L displayed weak cleavage activities (Figure 4).

DISCUSSION

Despite significant advances in the study of halogen X-bonding in material chemistry, these interactions are still underexploited for the design of potent and selective biomolecule ligands

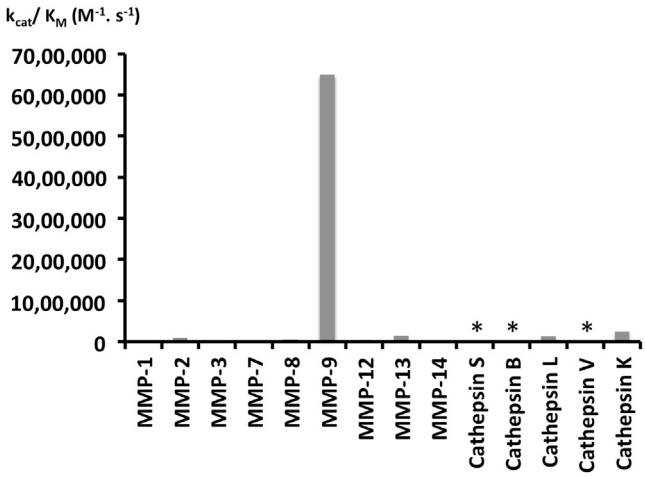

Figure 4. Catalytic Efficiency of a Set of Nine MMPs and Five Cathepsins for the Cleavage of Probe Substrate 8

For cathepsins labeled with an asterisk, no cleavage was observed. Experimental conditions: 50 mM Tris-HCl buffer, pH 6.8, 10 mM $CaCl_2$ at 25°C, 0.5 μM probe **8**, and 0.3 nM MMPs and cathepsins. Data are means ± SEM. See also Figure S2 and Tables S1 and S4.

(Scholfield et al., 2013). The tight directionality of these interactions and their thermodynamic stability may both be useful for drug design. The contributions of X-bonds to potency and selectivity have been reported for a small number of protein-ligand complexes. In many cases, these effects on potency are associated with the distance between X (halogen) and B (a negative site, like O) in R-X—B, as determined from crystal structures, being shorter than the sum of the X and B van der Waals radii (Baumli et al., 2010; Hardegger et al., 2011). Experimental data of this type are essential for validating computational approaches and for improving our understanding of these interactions. Fewer experimental data are available for halogen-water-hydrogen bridges than X-bonds, with only six relevant protein complex crystal structures being available; all involve an iodinated ligand in the Protein Data Bank (PDB), and the contribution of this interaction to the ligand affinity has not been quantified (Zhou et al., 2010). The interactions observed in the crystal structure of MMP-9:**8** complex are consistent with the presence of an I—O_w—H bridge. However, it should be noticed that the B-factor value of the water molecule involved in this bridge indicates a residual mobility, as at the Arg^{249} carbonyl group level, in comparison with the iodine atom B-factor value (Figure S1D). The structural differences observed between the complexes of probes **5** and **8** with MMP-9 indicate that the difference in the catalytic efficiency exhibited by MMP-9 when cleaving the probes may be due to a stabilizing contribution from the I—O_W—H bridge or the I—O_w halogen bond. If true, the 23-fold difference in the catalytic efficiency of MMP-9 toward probes **5** and **8** implies that these interactions correspond to a difference in free energy of 1.88 kcal/mol (ΔΔG) in the transition state structure stabilization between probes **5** and **8**. Although the MMP-9:**5** and MMP-9:**8** complexes with intact peptide bonds are not strictly equivalent to the transition-state structures, most differences between these two states should take place at the substrate backbone level, and less in the depth of the S_1' cavity, because side chain movements in the P_1' position are restricted by a narrowing at entrance of the cavity. Obviously, the contribution of additional factors cannot be excluded. It would be informative to determine why X-bonding or analogous I—O_W—H bridges are not operative in other MMPs, given that their S_1' cavities share many structural similarities. There may be local structural or dynamic reasons why the formation of specific interactions with iodine may be possible for probe **8** only in MMP-9; indeed, the residue in position 249 (Arg^{249} in MMP-9) is not conserved between MMPs and belongs to the S_1' loop, a loop being only poorly conserved between MMPs. Efforts to obtain crystal structures with other MMPs failed. For Glu → Ala mutants of both MMP-12 and MMP-8, products corresponding to cleavage of the substrate were observed in their active sites, suggesting that additional mutations are required to decrease residual MMP activity further. It would be useful to obtain thermodynamic data to determine energy differences (enthalpy and entropic contribution) for the formation of the complexes of MMP-9 with probes **5** and **8**. As recently reported, the entropic contributions to the total free energies may depend on the halogen (Carter et al., 2013). Here again, residual activity of the MMP-9 mutant in solution at 25°C has prevented us from obtaining the expected data.

SIGNIFICANCE

Our results suggest that halogen bonding could be exploited as a new avenue for developing probes or inhibitors with improved selectivity toward MMPs. Both direct and indirect halogen bonding should be explored, and the MMP structures reported here provide useful hints on how to achieve these objectives. The particular probe sequence used in this work for MMP-9, a key MMP involved in many human disorders (Vandooren et al., 2013), could also be used for various applications, including detection of MMP-9 activity in vitro and in vivo by imaging, by inserting this sequence into probes designed for such applications (Jiang et al., 2004; Ryu et al., 2013).

EXPERIMENTAL PROCEDURES

Peptide Synthesis and Characterization

Commercial reagents were used as received without additional purification. Solvents were of the reagent grade available. Fmoc amino acids, rink amide resin, universal polyethlene glycol (PEG) NovaTag resin, and 1-[(1-(cyano-2-ethoxy-2-oxoethylideneaminooxy) dimethylaminomorpholino)] uronium hexafluorophosphate (COMU) were from Novabiochem. *N*-α-Fmoc-*N*-β-(2,4-dinitrophenyl)-L-2,3-diaminopropionic acid, Fmoc-4- fluoro-L-phenylalanine, and (7-methoxycoumarin- 4-yl)acetyl were from Bachem. Fmoc-4-nitrophenylalanine, Fmoc-4-bromo-L-phenylalanine, Fmoc-4-chloro-L-phenylalanine, and Fmoc-4-(phenoxy)-L-phenylalanine were from PolyPeptide. Fmoc-4-iodo-L-phenylalanine, Fmoc-propargyl glycine, 1-hydroxybenzotriazole, dichloromethane (DCM), *N,N*-dimethylformamide (DMF), anhydrous tetrahydrofuran, phenylboronic acid, tetrakis(triphenylphosphine)palladium, 4-bromobiphenyle, sodium ascorbate, sodium azide, N,N-dimethylethylenediamine, copper iodide, 2-amino-2-(hydroxymethyl)-1,3-propanediol (Tris base), and calcium chloride ($CaCl_2$) were from Sigma-Aldrich. N,N-diisoproylethylamine (DIPEA) was from Fluka.

Analytical and preparative reverse-phase high-performance liquid chromatography (HPLC) separations were performed on a Shimadzu HPLC system using analytical AIT C8 Kromasil (250 × 4.6 mm; 100 Å; gradient, 0 to 20 min/0 to 100%B; flow rate, 1 ml · min^{-1}) and semipreparative AIT C8

Kromasil (250 × 20 mm; 100 Å; gradient, 0 to 30 min/0 to 100%B; flow rate, 3 ml · min^{-1}) columns; and UV detection was performed at 215 nm at 330 nm. Solvent systems used were as follows: A: 0.1% trifluoroacetic acid (TFA) in water; and B: 0.09% TFA in acetonitrile.

A 4800 spectrometer MALDI-TOF/TOF Proteomics Analyzer (Applied Biosystems) was used for mass spectrometry analysis of samples. α-Cyano-4-hydroxycinnamic acid from Fluka was used as the organic matrix for mass spectrometry analysis. Cyanine substrate was analyzed on a hybrid instrument LTQ-ORBITRAP-ThermoElectron Corporation. UV measurements were performed with a Shimadzu spectrophotometer (UV 1800).

Human MMPs (MMP-2, MMP-3, MMP-7, MMP-8, MMP-9, MMP-12, MMP-13, MMP-14) and human cathepsins B, L, S, and V were from R&D Systems; human cathepsin K was from Calbiochem. MMP activation was performed by treatment with *p*-aminophenylmercuric acid according to supplier indication.

Probe Synthesis

Probes were synthesized by Fmoc solid-phase synthesis strategy. Rink amide resin was swelled with DCM (15 min). Removal of Fmoc was performed using piperidine in DMF (20% piperidine, 2 × 2 min, 1 × 5 min), then Fmoc-Arg-OH was incorporated into the solid support, using COMU as a coupling agent for 30 min (6 equivalents of amino acid, 5.8 equivalents of COMU, 12 equivalents of DIPEA in DMF). A second coupling was performed for 20 min (3 equivalents of amino acid, 2.8 equivalents of COMU, 6 equivalents of DIPEA in DMF). After sequential incorporation of each amino acid, the fluorophore (7-methoxycoumarin-4-yl)acetyl was coupled (6 equivalents of amino acid, 5.8 equivalents of COMU, 12 equivalents of DIPEA in DMF) for 1 hr, and a second coupling was performed. After cleavage of the resin (TFA/triisopropylsilane/H_2O, 95/2.5/2.5, 4 hr) and freeze-drying of the cleavage solution, crude product was purified by HPLC (0%–100%B in 30 min). After freeze-drying of the purified fractions, DMSO was added and probe concentration was determined by UV (λ = 333 nm; ε = 21,470 cm^{-1} M^{-1}). The product purity was assessed by analytical HPLC and mass spectrometry analysis. Further details on synthesis and characterization of probes are provided in the Supplemental Information.

Enzyme Assays

Enzyme inhibition assays were carried out in 50 mM Tris-HCl buffer, pH 6.8, 10 mM $CaCl_2$, at 25°C. The assays were performed in black 96-well plates (nonbinding surface plates; Corning Costar Catalog No. 3651). Progress curves were monitored by recording the increase in fluorescence resulting from substrate cleavage ($\lambda_{excitation}$ = 320 nm, $\lambda_{emission}$ = 405 nm). The conditions of a typical experiment were 100 μl of buffer and 1–5 nM of MMP or cathepsins (R & R Systems). The reaction was then initiated by addition of 0.5 μM of substrate (stock solution of 100 μM of substrate in DMSO). Data were collected for 1 hr. The k_{cat}/K_M values were determined from first-order full-time reaction curves ($S << K_M$; S = 0.5 μM) and fitted with the integrated Michaelis-Menten equation by nonlinear regression: $P = S_0(1 - \exp(-kt))$, where P is product concentration; S_0 is substrate concentration at t (time) = 0; exp is exponential; k is (k_{cat}/K_M) · E; and E is enzyme concentration (Table S1). The kinetic parameters K_M and k_{cat} were estimated according to the direct linear plot method (Table S4).

Structural Studies

Protein Preparation

The expression and purification for the mostly inactive mini-MMP-9 catalytic domain (MMP-9, Glu^{227} → Ala^{227}, MMP-9A) used in the crystallographic studies has been described elsewhere (Antoni et al., 2013). In brief, the synthetic gene used for the catalytic domain of human MMP-9 comprises residues Gly106–Gly215 and Gln391–Gly444, without the fibronectin domains and with the catalytic glutamate mutated to alanine (Tochowicz et al., 2007). Plasmids were propagated in the *Escherichia coli* strain XL1-Blue, and the recombinant catalytic domains were expressed in *E. coli* BL21 (DE3 star) cells. After induction, the cells were harvested by centrifugation and the pellets were resuspended. The cell suspension was disrupted and then centrifuged. The pellets were washed and then dissolved again. Refolding, purification, and dialysis steps were carried out as described elsewhere (Antoni et al., 2013). Acetohydroxamic acid (AHA; 120 mM) was added to prevent self-degradation during concentration with an Amicon-stirred ultrafiltration cell with an ultrafiltration regenerated-cellulose disk membrane (3,500 Da molecular weight cut-off; Millipore). The enzyme was concentrated in the range of 0.182–0.421 mM in a buffer consisting of 3 mM $CaCl_2$, 120 mM AHA, 200 mM NaCl, 20 mM Tris-HCl, pH 7.5. By SDS-PAGE, the purity can be evaluated to be higher than 95%.

Crystallization and Structure Determination

The crystallization trials were carried out by sitting vapor diffusion with 1 μl equivolumetric drops of protein substrate and reservoir solution using CrysChem plates that were equilibrated in a cooled incubator at 20°C. Probe **8** was added with 1.8 stoichiometric excess (0.33 mM) to the enzyme at 0.182 mM used in the crystallization studies. The reservoir solution consisted of 10% PEG 20K, 100 mM MMT buffer (mixed L-malic acid, MES, and Tris in the ratio 1:2:2; 75% at pH 4 and 25% at pH 9), 800 mM NaCl, 200 mM $SrCl_2$, and 0.01% azide (Newman, 2004). Trials with probe **5** set up as for probe **8** gave crystals of the product complex. The complex of the intact substrate could be obtained when drops of probe **5** were streak seeded (Stura and Wilson, 1991) immediately after setting up the drops with crystals of probe **8** with the intact substrate, resulting in crystals that diffracted to only 2.7 Å. The diffraction limit could be increased to 1.85 Å with protein-inhibitor solution prepared with 0.42 mM MMP-9, 1 mM probe, 120 mM AHA, 17 mM $SrCl_2$, and 1% NaN_3 (Table S2). The crystals of the MMP-9A:probe **8** complex were transferred to a premixed cryo-protecting solution based on condition C2 from CryoProtX (Molecular Dimensions) (as described in Vera and Stura, 2013) for a few seconds, and then they were picked up into a loop and finally cryo-cooled in liquid nitrogen (Table S2). For the crystals of the MMP-9A:probe **5**, the best diffraction was obtained using a new evolution of the premixed solutions also including 5% dioxane (Table S2) picked up with a litho-loop mounted and flash-cooled in liquid nitrogen using magnetic SPINE-compatible cryovials for data collection at synchrotron facilities. Data for the MMP-9A-probe **8** complex were collected at the Soleil Synchrotron Facility on beamline Proxima 1 at 100 K from a single crystal and reduced using XDS (Kabsch, 2010) and the script "xdsme". The crystal belongs to the space group $P2_12_12_1$ with the following cell parameters: a = 34.2 Å, b = 57.4 Å, and c = 172.0 Å diffracting to 1.7 Å resolution (Table S2). The structure was solved by molecular replacement with MOLREP (Vagin and Teplyakov, 2010), using the coordinates of the cleaved complex and refined with REFMAC5 (Murshudov et al., 2011) and phenix.refine (Adams et al., 2010) to improve the solvent model. Restraints for the 7-methoxycoumarin-4-acetic acid and the (2S)-2-ammonio-4-[(2,4-dinitrophenyl)amino]propanoate probe components were created using the monomer library sketcher from the CCP4 program suite (Winn et al., 2011). The model was rebuilt in the electron density in COOT (Emsley et al., 2010). The data for the MMP-9A:probe **5** complex were collected at the European Synchrotron Radiation Facility, on beamline ID23-1 from a single crystal, and the data were processed automatically using XDS (Kabsch, 2010). The crystal belongs to the orthorhombic $P2_12_12_1$, with cell parameters almost identical to those of crystals of MMP-9A:probe **8** (Table S2). Being isomorphous with the crystal structure of probe **8** in complex with MMP-9, after rigid body refinement with REFMAC5 (Murshudov et al., 2011) and the replacement of the iodophenyl by a fluorophenyl moiety, the structure was improved with cycles in phenix.refine (Adams et al., 2010) and COOT. The electron density for the substrate in both molecules in the asymmetric unit is well defined.

Crystallization Strategies

Several crystallization attempts were carried out over a period of more than 12 months before high-resolution X-ray structures could be obtained with both intact substrates. Although the catalytic glutamate has been mutated to alanine, the enzyme remained catalytically competent over the period of 1–4 days needed to grow large crystals suitable for crystallographic studies. High concentrations of AHA (120 mM) were found to be relatively ineffective to prevent cleavage. Success was achieved with probe **8** when strontium was added to the crystallization precipitant so that it could replace partially two of the more labile calcium ions that contribute to enzyme stabilization. The same strategy allowed data to be collected for probe **5** but only to 2.7 Å, probably because of the heterogeneous presence of the cleavage product. The resolution could be improved to 1.85 Å after NaN_3 was added to the protein-substrate mix before crystallization.

ACCESSION NUMBERS

The crystal structure data for the MMP-9 in complex with probe **8** and probe **5** are deposited in PDB under accession codes 4JIJ and 4JQG, respectively.

SUPPLEMENTAL INFORMATION

Supplemental Information includes Supplemental Experimental Procedures, two figures, and four tables and can be found with this article online at http://dx.doi.org/10.1016/j.chembiol.2014.01.008.

ACKNOWLEDGMENTS

This work was supported by the European FP7 Health Program "Livimode" (2009, 241919) and the Commissariat à l'Energie Atomique. This work is dedicated to Professor Athanasios Yiotakis on the occasion of his 71st birthday.

Received: July 26, 2013
Revised: January 7, 2014
Accepted: January 13, 2014
Published: February 27, 2014

REFERENCES

Adams, P.D., Afonine, P.V., Bunkóczi, G., Chen, V.B., Davis, I.W., Echols, N., Headd, J.J., Hung, L.W., Kapral, G.J., Grosse-Kunstleve, R.W., et al. (2010). PHENIX: a comprehensive Python-based system for macromolecular structure solution. Acta Crystallogr. D Biol. Crystallogr. *66*, 213–221.

Akers, W.J., Xu, B., Lee, H., Sudlow, G.P., Fields, G.B., Achilefu, S., and Edwards, W.B. (2012). Detection of MMP-2 and MMP-9 activity in vivo with a triple-helical peptide optical probe. Bioconjug. Chem. *23*, 656–663.

Antoni, C., Vera, L., Devel, L., Catalani, M.P., Czarny, B., Cassar-Lajeunesse, E., Nuti, E., Rossello, A., Dive, V., and Stura, E.A. (2013). Crystallization of bi-functional ligand protein complexes. J. Struct. Biol. *182*, 246–254.

Auffinger, P., Hays, F.A., Westhof, E., and Ho, P.S. (2004). Halogen bonds in biological molecules. Proc. Natl. Acad. Sci. USA *101*, 16789–16794.

Baumli, S., Endicott, J.A., and Johnson, L.N. (2010). Halogen bonds form the basis for selective P-TEFb inhibition by DRB. Chem. Biol. *17*, 931–936.

Carter, M., Voth, A.R., Scholfield, M.R., Rummel, B., Sowers, L.C., and Ho, P.S. (2013). Enthalpy-entropy compensation in biomolecular halogen bonds measured in DNA junctions. Biochemistry *52*, 4891–4903.

Devel, L., Czarny, B., Beau, F., Georgiadis, D., Stura, E., and Dive, V. (2010). Third generation of matrix metalloprotease inhibitors: Gain in selectivity by targeting the depth of the S1′ cavity. Biochimie *92*, 1501–1508.

Emsley, P., Lohkamp, B., Scott, W.G., and Cowtan, K. (2010). Features and development of Coot. Acta Crystallogr. D Biol. Crystallogr. *66*, 486–501.

Fanjul-Fernández, M., Folgueras, A.R., Cabrera, S., and López-Otín, C. (2010). Matrix metalloproteinases: evolution, gene regulation and functional analysis in mouse models. Biochim. Biophys. Acta *1803*, 3–19.

Fingleton, B. (2007). Matrix metalloproteinases as valid clinical targets. Curr. Pharm. Des. *13*, 333–346.

Fu, X., Parks, W.C., and Heinecke, J.W. (2008). Activation and silencing of matrix metalloproteinases. Semin. Cell Dev. Biol. *19*, 2–13.

Hardegger, L.A., Kuhn, B., Spinnler, B., Anselm, L., Ecabert, R., Stihle, M., Gsell, B., Thoma, R., Diez, J., Benz, J., et al. (2011). Halogen bonding at the active sites of human cathepsin L and MEK1 kinase: efficient interactions in different environments. ChemMedChem *6*, 2048–2054.

Jabaiah, A., and Daugherty, P.S. (2011). Directed evolution of protease beacons that enable sensitive detection of endogenous MT1-MMP activity in tumor cell lines. Chem. Biol. *18*, 392–401.

Jiang, T., Olson, E.S., Nguyen, Q.T., Roy, M., Jennings, P.A., and Tsien, R.Y. (2004). Tumor imaging by means of proteolytic activation of cell-penetrating peptides. Proc. Natl. Acad. Sci. USA *101*, 17867–17872.

Kabsch, W. (2010). Integration, scaling, space-group assignment and post-refinement. Acta Crystallogr. D Biol. Crystallogr. *66*, 133–144.

Kridel, S.J., Chen, E., Kotra, L.P., Howard, E.W., Mobashery, S., and Smith, J.W. (2001). Substrate hydrolysis by matrix metalloproteinase-9. J. Biol. Chem. *276*, 20572–20578.

Morrison, C.J., Butler, G.S., Rodríguez, D., and Overall, C.M. (2009). Matrix metalloproteinase proteomics: substrates, targets, and therapy. Curr. Opin. Cell Biol. *21*, 645–653.

Mott, J.D., and Werb, Z. (2004). Regulation of matrix biology by matrix metalloproteinases. Curr. Opin. Cell Biol. *16*, 558–564.

Murshudov, G.N., Skubák, P., Lebedev, A.A., Pannu, N.S., Steiner, R.A., Nicholls, R.A., Winn, M.D., Long, F., and Vagin, A.A. (2011). REFMAC5 for the refinement of macromolecular crystal structures. Acta Crystallogr. D Biol. Crystallogr. *67*, 355–367.

Newman, J. (2004). Novel buffer systems for macromolecular crystallization. Acta Crystallogr. D Biol. Crystallogr. *60*, 610–612.

Parisini, E., Metrangolo, P., Pilati, T., Resnati, G., and Terraneo, G. (2011). Halogen bonding in halocarbon-protein complexes: a structural survey. Chem. Soc. Rev. *40*, 2267–2278.

Parks, W.C., Wilson, C.L., and López-Boado, Y.S. (2004). Matrix metalloproteinases as modulators of inflammation and innate immunity. Nat. Rev. Immunol. *4*, 617–629.

Politzer, P., and Murray, J.S. (2013). Halogen bonding: an interim discussion. ChemPhysChem *14*, 278–294.

Politzer, P., Murray, J.S., and Clark, T. (2010). Halogen bonding: an electrostatically-driven highly directional noncovalent interaction. Phys. Chem. Chem. Phys. *12*, 7748–7757.

Ryu, J.H., Shin, J.Y., Kim, S.A., Kang, S.W., Kim, H., Kang, S., Choi, K., Kwon, I.C., Kim, B.S., and Kim, K. (2013). Non-invasive optical imaging of matrix metalloproteinase activity with albumin-based fluorogenic nanoprobes during angiogenesis in a mouse hindlimb ischemia model. Biomaterials *34*, 6871–6881.

Scholfield, M.R., Zanden, C.M., Carter, M., and Ho, P.S. (2013). Halogen bonding (X-bonding): a biological perspective. Protein Sci. *22*, 139–152.

Sternlicht, M.D., and Werb, Z. (2001). How matrix metalloproteinases regulate cell behavior. Annu. Rev. Cell Dev. Biol. *17*, 463–516.

Stura, E.A., and Wilson, I.A. (1991). Applications of of the streak seeding technique in protein crystallization. J. Cryst. Growth *110*, 270–282.

Tochowicz, A., Maskos, K., Huber, R., Oltenfreiter, R., Dive, V., Yiotakis, A., Zanda, M., Pourmotabbed, T., Bode, W., and Goettig, P. (2007). Crystal structures of MMP-9 complexes with five inhibitors: contribution of the flexible Arg424 side-chain to selectivity. J. Mol. Biol. *371*, 989–1006.

Vagin, A., and Teplyakov, A. (2010). Molecular replacement with MOLREP. Acta Crystallogr. D Biol. Crystallogr. *66*, 22–25.

Vandooren, J., Van den Steen, P.E., and Opdenakker, G. (2013). Biochemistry and molecular biology of gelatinase B or matrix metalloproteinase-9 (MMP-9): the next decade. Crit. Rev. Biochem. Mol. Biol. *48*, 222–272.

Vera, L., and Stura, E.A. (2013). Strategies for protein cryocrystallography. Cryst. Growth & Des. *13*, 1878–1888.

Verdoes, M., Oresic Bender, K., Segal, E., van der Linden, W.A., Syed, S., Withana, N.P., Sanman, L.E., and Bogyo, M. (2013). Improved quenched fluorescent probe for imaging of cysteine cathepsin activity. J. Am. Chem. Soc. *135*, 14726–14730.

Winn, M.D., Ballard, C.C., Cowtan, K.D., Dodson, E.J., Emsley, P., Evans, P.R., Keegan, R.M., Krissinel, E.B., Leslie, A.G., McCoy, A., et al. (2011). Overview of the CCP4 suite and current developments. Acta Crystallogr. D Biol. Crystallogr. *67*, 235–242.

Yiotakis, A., and Dive, V. (2008). Synthetic active site-directed inhibitors of metzincins: achievement and perspectives. Mol. Aspects Med. *29*, 329–338.

Zhou, P., Lv, J., Zou, J., Tian, F., and Shang, Z. (2010). Halogen-water-hydrogen bridges in biomolecules. J. Struct. Biol. *169*, 172–182.